Design Optimization of Interdigital Filters Using Aggressive Space Mapping and Decomposition

John W. Bandler, *Fellow, IEEE,* Radoslaw M. Biernacki, *Fellow, IEEE,*
Shao Hua Chen, *Senior Member, IEEE,* and Ya Fei Huang, *Member, IEEE*

Abstract— This paper presents a new electromagnetic (EM) design methodology which combines two powerful techniques in a coherent strategy: space mapping (SM) and decomposition. An accurate but computationally intensive fine-resolution EM model is used sparingly only to calibrate a less accurate, but computationally much more efficient "coarse model." Applying this new approach to interdigital filter design, the authors exploit structural decomposition to construct a highly efficient coarse model using a combination of EM models with a coarse grid and empirical models for the noncritical substructures. The authors employ the aggressive SM optimization technique to obtain a rapidly improved design after each fine-model simulation while the bulk of the computation is carried out using the coarse model. To avoid possible oscillation in the iterative process, a penalty function is introduced. Fast and stable convergence to a desirable interdigital filter design is achieved after only three EM fine-model simulations.

Index Terms— Design automation, electromagnetic analysis, microstrip circuits, microwave filters, optimization methods.

I. INTRODUCTION

INTERDIGITAL filters have the advantage of compact size and adaptability to narrow- and wide-band applications. Pioneering work [1]–[3] in this field first focused on synthesis techniques. Tapped lines were later introduced [4], [5] at the input and output resonators to offer both space and cost savings over the earlier designs by eliminating the first and the last end sections. An additional advantage is that the tapped structure can realize very weak couplings when the traditional structure becomes impractical. Unfortunately, exact synthesis of tapped line filters is not straightforward. Available techniques are not directly applicable to microstrip configurations. Final validation using rigorous models is considered necessary.

The method of moments (MoM) [6], [7] and the finite-element method (FEM) [8] have been used successfully for EM field analysis in two-dimensional (2-D) and three-dimensional (3-D) structures. They offer excellent accuracy if critical areas are meshed with a sufficiently small grid. One major disadvantage with these numerical techniques is their heavy demand on computer resources. It is commonly perceived that iterative optimization methods would require too many EM simulations and consequently consume excessive central processing unit (CPU) time. For this reason, the practical utilization of EM simulators is often limited to design validation.

This paper presents a new design methodology which combines two powerful techniques in a coherent strategy: space mapping (SM) and decomposition. The decomposition technique partitions a complex structure into a few smaller substructures [9]–[11]. Each of them is analyzed separately and the results are combined to obtain the response of the overall structure. More efficiently, 2-D analytical methods or even empirical formulas can be used for the calculation of some noncritical regions while full-wave 3-D models are adopted for the analysis of the key substructures. Couplings between the decomposed substructures are neglected, therefore, some loss of accuracy is expected.

The other cornerstone of the authors' methodology is the SM concept which has aroused excitement and increasing attention as a fundamental new theory in engineering-oriented optimization practice [12]–[14]. An accurate but computationally intensive fine-resolution EM model is used sparingly only to calibrate a less accurate, but computationally much more efficient coarse model. A mapping is established between two spaces, namely, between the coarse model and the fine model. The aggressive SM algorithm incorporates a quasi-Newton iteration with first-order derivative updates using the classic Broyden formula [15]. A rapidly improved design is expected to be obtained after each fine-model simulation while the bulk of the computation involved in optimization is carried out in the coarse model space. This is much more efficient than a "brute force" optimization directly driving fine-model EM simulations.

Parameter extraction is a crucial step in the SM algorithm. If the parameter extraction result is not unique, it can lead to oscillation in the iterative process. To avoid such a possibility, a penalty function is introduced in conjunction with the Huber or ℓ_1 objective function [16], [17].

The new approach discussed here is applied to the design optimization of an interdigital filter, driving a well-recognized

EM simulator (**em** [18]). Fast and stable convergence to a desirable filter design is achieved after only three EM fine-model simulations.

II. AGGRESSIVE SPACE MAPPING

A. Basic Concept

Consider models in two distinct spaces: the EM space, denoted by $\boldsymbol{X}_{\text{em}}$, and the optimization space, denoted by $\boldsymbol{X}_{\text{os}}$. The $\boldsymbol{X}_{\text{em}}$ model is called a fine model, assuming that it is rigorous and accurate, but its simulation is CPU intensive. In contrast, the $\boldsymbol{X}_{\text{os}}$ model is less accurate but faster to compute, hence it is called a coarse model. For instance, the $\boldsymbol{X}_{\text{em}}$ model can be a mode-matching model with an adequately large number of modes or a FEM model with a sufficiently small mesh size. The models in $\boldsymbol{X}_{\text{os}}$ may include empirical models, equivalent circuits and EM models with a coarse grid size.

The designable model parameters in $\boldsymbol{X}_{\text{em}}$ and $\boldsymbol{X}_{\text{os}}$ are denoted by $\boldsymbol{x}_{\text{em}}$ and $\boldsymbol{x}_{\text{os}}$, respectively. Typically, gradient-based optimization algorithms assume that the variables are continuous. To reconcile this assumption with an EM simulator which discretizes geometrical dimensions, linear and quadratic interpolation techniques are applied [19].

One wishes to find a mapping $\boldsymbol{P}$ between the two spaces

$$\boldsymbol{x}_{\text{os}} = \boldsymbol{P}(\boldsymbol{x}_{\text{em}}) \tag{1}$$

such that

$$\boldsymbol{R}_{\text{os}}(\boldsymbol{P}(\boldsymbol{x}_{\text{em}})) \approx \boldsymbol{R}_{\text{em}}(\boldsymbol{x}_{\text{em}}) \tag{2}$$

or more precisely,

$$\|\boldsymbol{R}_{\text{os}}(\boldsymbol{x}_{\text{os}}) - \boldsymbol{R}_{\text{em}}(\boldsymbol{x}_{\text{em}})\| \leq \varepsilon \tag{3}$$

where $\|\cdot\|$ denotes the Huber or ℓ_1 norm and ε is a small positive constant. $\boldsymbol{R}_{\text{em}}(\boldsymbol{x}_{\text{em}})$ and $\boldsymbol{R}_{\text{os}}(\boldsymbol{x}_{\text{os}})$ represent the responses of the fine model and the coarse model, respectively.

The aim here is to avoid direct optimization in the CPU-intensive $\boldsymbol{X}_{\text{em}}$ space. Instead, the bulk of the computation involved in optimization is carried out in the $\boldsymbol{X}_{\text{os}}$ space. The optimal solution in $\boldsymbol{X}_{\text{os}}$ can then be mapped to $\boldsymbol{X}_{\text{em}}$ using an inverse mapping $\boldsymbol{P}^{-1}$ derived from (1).

In the aggressive SM procedure, the mapping function is updated through a quasi-Newton iteration with first-order derivative approximations based on the classic Broyden formula [15]. The detailed description of this algorithm can be found in [13].

B. Parameter Extraction and Penalty Function

Denoting the optimal solution in $\boldsymbol{X}_{\text{os}}$ by $\boldsymbol{x}_{\text{os}}^*$, one starts with $\boldsymbol{x}_{\text{em}}^{(1)} = \boldsymbol{x}_{\text{os}}^*$. At the ith iteration, one simulates the $\boldsymbol{X}_{\text{em}}$ model at $\boldsymbol{x}_{\text{em}}^{(i)}$ and obtains $\boldsymbol{x}_{\text{os}}^{(i)}$ by parameter extraction

$$\underset{\boldsymbol{x}_{\text{os}}^{(i)}}{\text{minimize}} \ \|\boldsymbol{R}_{\text{os}}(\boldsymbol{x}_{\text{os}}^{(i)}) - \boldsymbol{R}_{\text{em}}(\boldsymbol{x}_{\text{em}}^{(i)})\|. \tag{4}$$

Then, the mapping $\boldsymbol{P}_i$ is updated by the Broyden formula and used to produce the following iterate:

$$\boldsymbol{x}_{\text{em}}^{(i+1)} = \boldsymbol{P}_i^{-1}(\boldsymbol{x}_{\text{os}}^*). \tag{5}$$

The uniqueness of the parameter extraction is crucial. If the solution of (4) is not unique, the SM process may be slow to converge, oscillate, or fail to converge at all.

To address this problem, a penalty function is introduced and modifies (4) as

$$\underset{\boldsymbol{x}_{\text{os}}^{(i)}}{\text{minimize}} \ H(\boldsymbol{x}_{\text{os}}^{(i)}, w) = \|\boldsymbol{R}_{\text{os}}(\boldsymbol{x}_{\text{os}}^{(i)}) - \boldsymbol{R}_{\text{em}}(\boldsymbol{x}_{\text{em}}^{(i)})\|$$
$$+ w\|\boldsymbol{x}_{\text{os}}^{(i)} - \boldsymbol{x}_{\text{os}}^*\| \tag{6}$$

where w is a nonnegative weighting factor.

The convergence of the SM process can be characterized as

$$\boldsymbol{x}_{\text{os}}^{(i)} \rightarrow \boldsymbol{x}_{\text{os}}^* \tag{7}$$

$$\boldsymbol{x}_{\text{em}}^{(i)} \rightarrow \overline{\boldsymbol{x}}_{\text{em}} \tag{8}$$

where $\overline{x}_{\text{em}}$ represents the desired SM solution in $\boldsymbol{X}_{\text{em}}$.

In effect, the penalty terms in (6) are used to force its solution toward satisfying (7). In situations where multiple solutions for the original parameter extraction problem (4) exist, the solution which is closest to satisfying (7) is favored.

With the penalty terms, the mapping derived from the solution of (6) is likely to be different from the mapping derived from the solution of (4). In this respect, the weighting factor w in (6) merits careful consideration. If w is too large, the result of the parameter extraction may not be very accurate in the sense that it may produce a poor agreement between $R_{\text{os}}(\boldsymbol{x}_{\text{os}}^{(i)})$ and $R_{\text{em}}(\boldsymbol{x}_{\text{em}}^{(i)})$. If w is too small, it may not achieve the intended purpose of forcing (7).

One can also see that as $\boldsymbol{x}_{\text{os}}^{(i)}$ converges to $\boldsymbol{x}_{\text{os}}^*$, the effect of the penalty terms gradually diminishes. In other words, the role of the penalty terms is most significant in the initial stage of the SM process, when nonunique parameter extraction results are most likely to occur. It is found that a suitable value for w is between 0.05 and 0.2 for the interdigital filter design considered.

C. Automated SM Optimization

The fully automated aggressive SM strategy is illustrated by the flowchart in Fig. 1. $\boldsymbol{x}_{\text{em}}^{(i+1)}$ in (5) can be expressed as

$$\boldsymbol{x}_{\text{em}}^{(i+1)} = \boldsymbol{x}_{\text{em}}^{(i)} + h^{(i)} \tag{9}$$

where $\boldsymbol{h}^{(i)}$ is the incremental vector computed by the SM algorithm in the ith iteration.

Since an EM simulator with a fixed discretization grid is used, the $\boldsymbol{X}_{\text{em}}$ model parameters need to be snapped to the grid. Assuming that $\boldsymbol{h}^{(i)}$ is the incremental vector calculated by the SM algorithm, one denotes by $\boldsymbol{h}^{(i)\prime}$ the vector after snapping to the grid. It can be expressed as

$$\boldsymbol{h}^{(i)\prime} = [k_1^{(i)}\Delta x_1, \, k_2^{(i)}\Delta x_2, \, \cdots, \, k_n^{(i)}\Delta x_n] \tag{10}$$

where

$$k_j^{(i)} = floor\left[\frac{h_j^{(i)}}{\Delta x_j} + \frac{1}{2}\right], \qquad j = 1, 2, \cdots, n \tag{11}$$

n is the number of the model parameters, Δx_j is the grid size of the jth parameter, and $h_j^{(i)}$ is the jth component of $\boldsymbol{h}^{(i)}$.
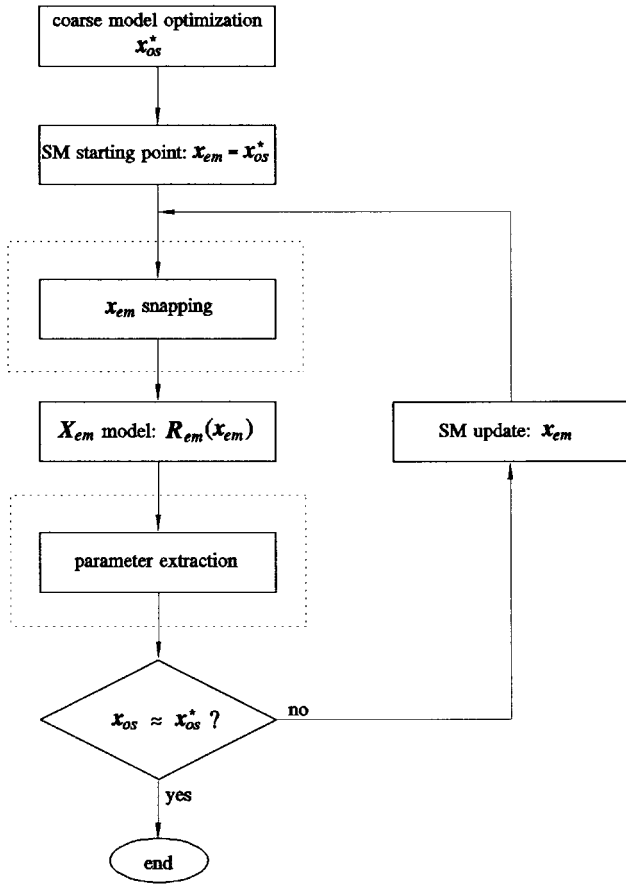
Fig. 1. Flowchart of the automated aggressive SM strategy.

Fig. 2. Detail of the x_{em} grid snapping step of Fig. 1.

Fig. 3. Detail of the parameter extraction loop of Fig. 1.

In the flowchart of Fig. 1, the vector $h^{(i)}$ is calculated within the "SM update" block. The calculation of $h^{(i)'}$ by (10) and (11) is implemented in the "x_{em} snapping" block, with further details shown in Fig. 2. With the consideration of snapping parameters to the grid, in this implementation (9) is replaced by

$$x_{\mathrm{em}}^{(i+1)} = x_{\mathrm{em}}^{(i)} + h^{(i)'}. \qquad (12)$$

If the X_{em} model has been simulated previously at $x_{\mathrm{em}}^{(i+1)}$, then the results are retrieved from the database. Otherwise a full-wave EM analysis is performed at $x_{\mathrm{em}}^{(i+1)}$.

Fig. 3 shows the details of the parameter extraction step.

III. THE FILTER MODELS AND DECOMPOSITION

A five-pole interdigital filter is shown in Fig. 4. The filter consists of five quarter-wavelength resonators, as well as input and output microstrip T-junctions within a shielded box. Each resonator is formed by one quarter-wavelength microstrip line section, shorted by a via at one end and opened at the other end. The arrows in Fig. 4 indicate the input and output reference planes, and the triangles symbolize the grounded vias. Some relevant material parameters and geometrical dimensions are listed in Table I.
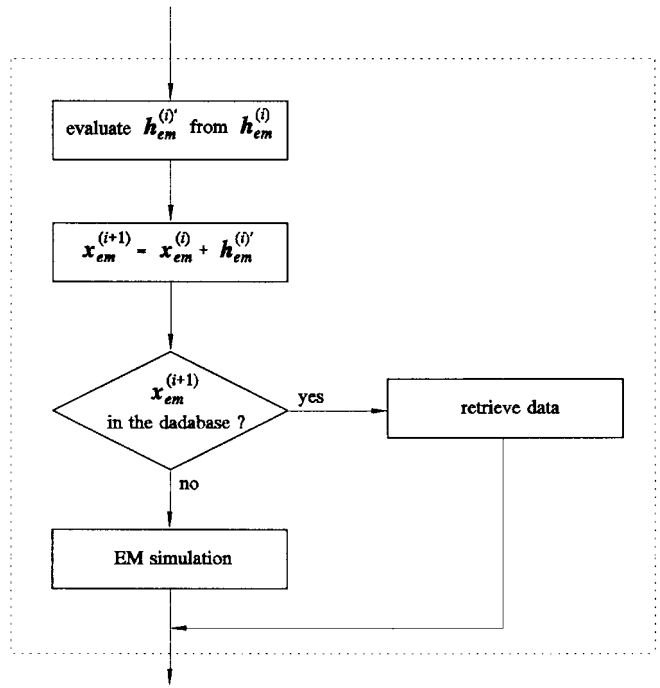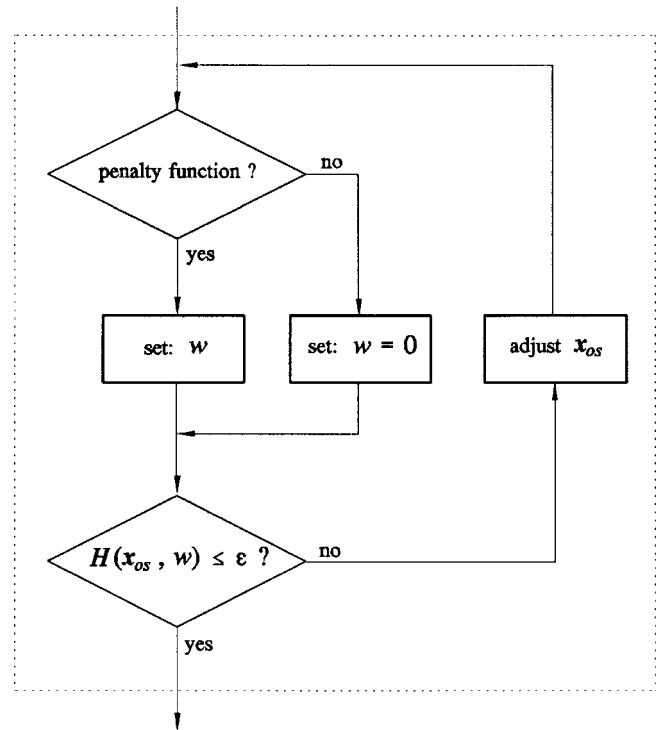
A. The Fine Model

For an accurate analysis of the interdigital filter using the full-wave MoM simulator *em* [18], a fine grid is needed to model the geometry precisely.

For the fine model in the SM process, the authors chose to simulate the complete filter structure as a whole with the grid size of 1×1 mil. With this grid size, the EM simulation

TABLE I
MATERIAL AND PHYSICAL PARAMETERS FOR THE FINE AND COARSE MODELS

Model Parameter	Fine Model	Coarse Model
substrate dielectric constant	9.8	9.8
substrate dielectric loss tangent	0/0.001*	0
substrate thickness (mil)	15	15
shielding cover height (mil)	75	75
conducting metal thickness (mil)	0	0
conductivity of the metal (copper)	$\infty/5.8\times10^{7*}$	∞
width of each resonator (mil)	10	10
width of input and output lines (mil)	10	10
x-grid size (mil) (whole structure)	1	–
y-grid size (mil) (whole structure)	1	–
x-grid size (mil) (via)	–	1
y-grid size (mil) (via)	–	1
diameter (mil) (via)	13	13
pad dimensions (mil × mil) (via)	25 × 25	25 × 25
x-grid size (mil) (12-port network)	–	5
y-grid size (mil) (12-port network)	–	10
l (mil) (12-port network)	–	180

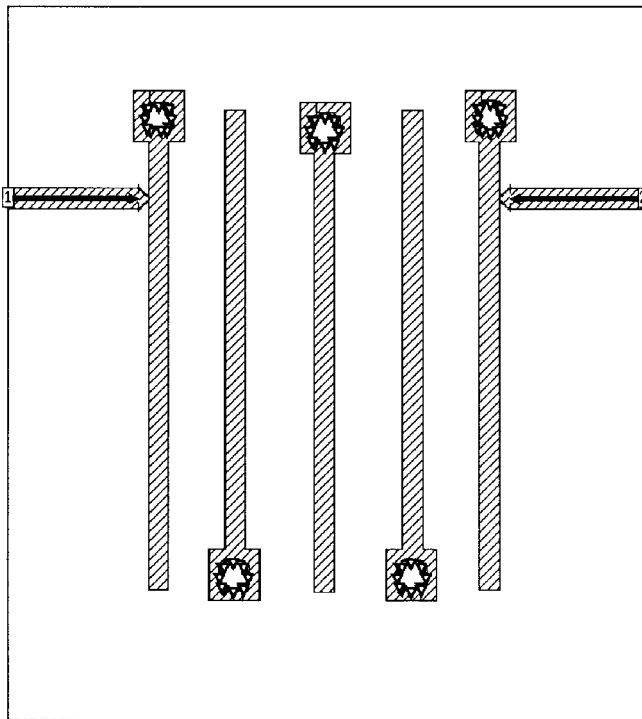* For the fine model, the values of loss tangent and conductivity are for simulations without and with losses, respectively.
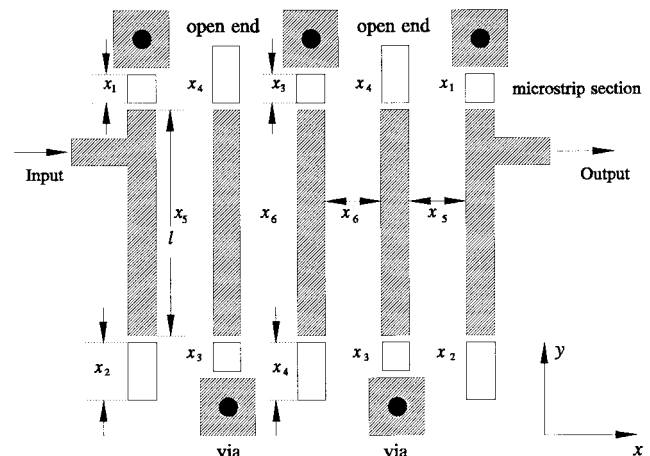

Fig. 4. A five-pole interdigital filter.

Fig. 5. A coarse model of the interdigital filter using decomposition.

that a "brute force" approach of directly driving the fine-model EM simulation within an iterative optimization process would require an excessive amount of CPU time.

B. Decomposition and the Coarse Model

Decomposition is used to construct an efficient coarse model for the SM optimization. As shown in Fig. 5, the filter is decomposed into a 12-port center piece, the vias, the microstrip line sections and the open ends. Referring to Fig. 5, the center shaded 12-port is analyzed by *em* with a very coarse
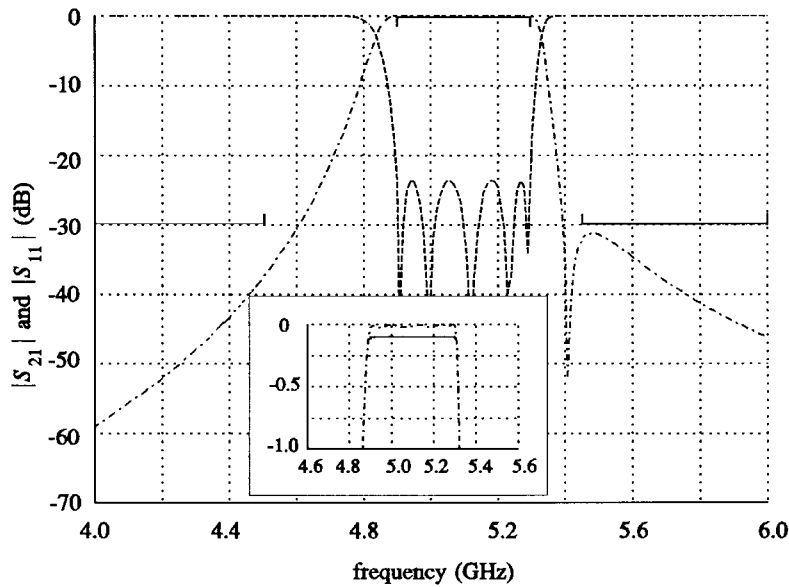
time is about 1.5 CPU h per frequency point on a Sun SPARCstation 10 (longer if losses are included). This means

Fig. 6. The interdigital filter responses after synthesis and minimax optimization using the coarse model ($\cdot$ $\cdot$ $\cdot$ $|S_{21}|$, $\cdot$ $\cdot$ $\cdot$ $|S_{11}|$). The insert shows the details of the passband.

grid: 5×10 mil. Off-grid responses, when needed during optimization, are obtained by linear or quadratic interpolation. The via is analyzed by *em* with a grid of 1×1 mil. All the other parts including the microstrip line sections and the open ends are analyzed using the empirical models in OSA90/hope [19]. The results are then connected through circuit theory to obtain the responses of the overall filter. Some relevant parameters of the coarse model are summarized in Table I.

Since the coarse model retains most of the adjacent and nonadjacent couplings, it provides reasonably accurate results at dramatically faster speed: the coarse model simulation takes less than 1 CPU min per frequency point on a Sun SPARCstation 10. Furthermore, by using a very coarse grid instead of a fine grid, much fewer full-wave EM simulations are needed during optimization. The overall CPU time required for optimizing the coarse model is about 2 h, which is of the same order of magnitude as the fine-model EM simulation at a single frequency point.

C. Optimization Variables

Using the geometry capture feature of *Empipe* [19], the authors define six optimization variables for the interdigital filter, shown in Fig. 5 as x_1, x_2, $\cdots$, x_6. These include the gaps between the resonators and lengths of the microstrip lines. The tapped positions of the input and output resonators are controlled indirectly by variables x_1 and x_2.

For the 12-port in the coarse model, the length l of each parallel microstrip section is fixed at 180 mil (about 70% of a quarter wavelength). The actual overall lengths of the resonators are determined by l and the variables x_1, x_2, x_3, and x_4. The gaps between the resonators are optimizable and the initial values are determined by synthesis. The authors also impose reasonable bounds on the gaps during optimization: 20 mil $\leq x_5 \leq$ 30 mil and 25 mil $\leq x_6 \leq$ 35 mil.

The dimensions of the vias are fixed.

IV. SM OPTIMIZATION OF THE INTERDIGITAL FILTER

A. Coarse Model Synthesis and Optimization

The interdigital filter design specifications are as follows:

center frequency	5.1 GHz
bandwidth	0.4 GHz
passband ripple	0.1 dB
isolation	30 dB
isolation bandwidth	0.95 GHz.

Following well-established synthesis techniques [20], the order of the filter is determined to be five. The authors chose 15-mil-thick alumina substrate with $\varepsilon_r = 9.8$. The width of each microstrip is chosen to be 10 mil for a good quality factor. The length of each resonator is initially set to a quarter wavelength. The gaps and the positions of the tapped lines are designed using synthesis techniques.

Using the synthesized design as a starting point, minimax optimization is performed on the coarse model. The optimal responses shown in Fig. 6 satisfy the specifications very well. The passband ripples are less than 0.1 dB. In the coarse model simulation, the 12-port substructure and the vias are analyzed by *em* at 51 frequency points.

B. Fine-Model SM Optimization for the Lossless Case

Using the optimal coarse model responses as the target, the aim is to find the SM solution in the fine-model space. Initially, the fine model without losses is considered.

Denoting the optimal coarse model by variables x_{os}^*, the aggressive SM process is started with $x_{em}^{(1)} = x_{os}^*$. The fine-model EM simulation results at the starting point are shown in Fig. 7. Not surprisingly, the fine-model responses deviate significantly from the optimal coarse-model responses. The passband return loss is only about 11 dB. Also, notice that in the lower stopband near 4.7 GHz the insertion loss is about 7.5 dB, which means the bandwidth is widened. This is most likely
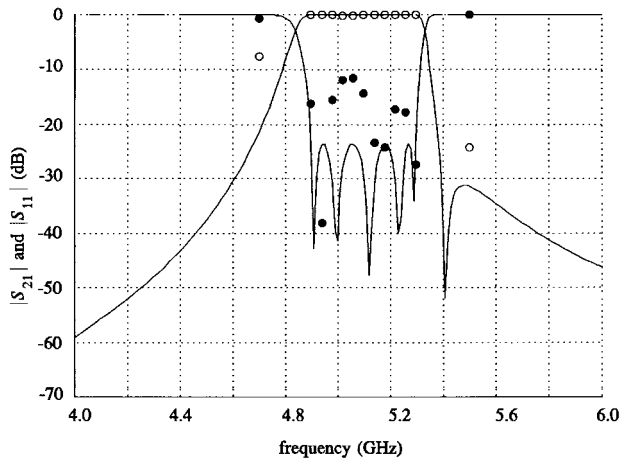
Fig. 7.   The solid lines represent the optimal $|S_{11}|$ and $|S_{21}|$ responses of the coarse model at x_{os}^*. The circles represent the fine-model responses at $x_{\text{em}}^{(1)} = x_{\text{os}}^*$ (o o o $|S_{21}|$, • • • $|S_{11}|$).

Fig. 9.   The fine-model responses (o o o $|S_{21}|$, • • • $|S_{11}|$) at $x_{\text{em}}^{(2)}$ after the first aggressive SM iteration. The solid lines represent the optimal $|S_{11}|$ and $|S_{21}|$ responses of the coarse model at x_{os}^*.
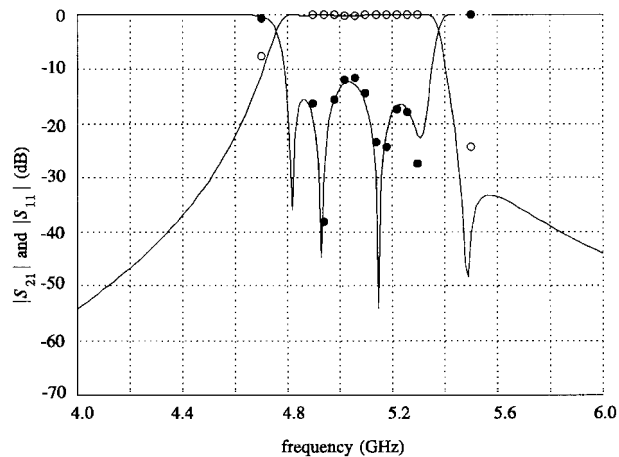

Fig. 8.   The parameter extraction results. The solid lines represent the coarse model responses at $x_{\text{os}}^{(1)}$. The circles represent the fine-model responses at $x_{\text{em}}^{(1)}$ (o o o $|S_{21}|$, • • • $|S_{11}|$).

Fig. 10.   The fine-model responses (o o o $|S_{21}|$, • • • $|S_{11}|$) at $x_{\text{em}}^{(3)}$ after the second aggressive SM iteration. The solid lines represent the optimal $|S_{11}|$ and $|S_{21}|$ responses of the coarse model at x_{os}^*.

TABLE II
ITERATIONS IN THE X_{os} SPACE

	x_1	x_2	x_3	x_4	x_5	x_6	Euclidian Distance
x_{os}^*	12.9745	26.9189	6.5706	27.6800	24.9709	30.2267	
$x_{os}^{(1)}$	13.3029	26.9011	6.6660	28.0791	22.2091	27.0548	4.28
$x_{os}^{(2)}$	13.1242	27.0223	6.7112	28.0204	24.7694	29.0795	1.17
$x_{os}^{(3)}$	13.0720	27.0985	6.7451	27.9848	24.7430	29.6345	0.76

All values shown are in mils.

due to the fact that some of the couplings between resonators are not taken into account by the coarse model.

The next step is to find a point in the X_{os} space, denoted by $x_{\text{os}}^{(1)}$, to match the responses of $x_{\text{em}}^{(1)}$ by parameter extraction with the penalty terms as defined in (6). The weighting factor for the penalty terms is chosen to be 0.15. The parameter extraction results are shown in Fig. 8. This process does not require any additional EM simulation of the fine model. Only the coarse model simulations are involved.

Based on the parameter values of $x_{\text{em}}^{(1)}$ and $x_{\text{os}}^{(1)}$, the mapping function is updated (the initial mapping is set to the identity mapping). Details of the updating formulas can be found in [13]. The inverse mapping of x_{os}^* leads to a new point in the X_{em} space: $x_{\text{em}}^{(2)}$. This completes one iteration of the aggressive SM strategy.

The fine-model EM simulation results of $x_{\text{em}}^{(2)}$ are shown in Fig. 9. It shows significant improvement over the starting point. Two major accomplishments are achieved in this one iteration. The scattered points of the return loss have been
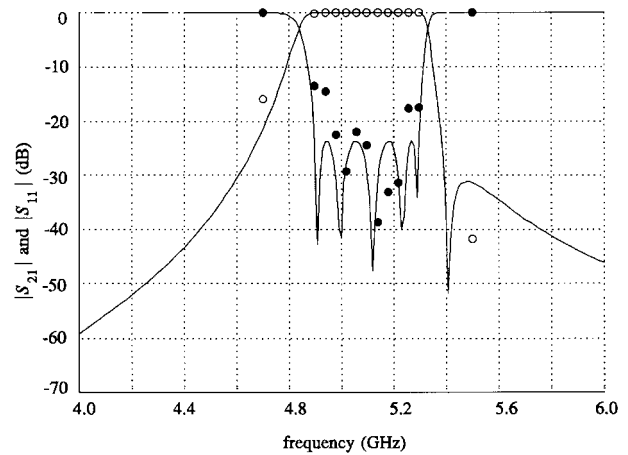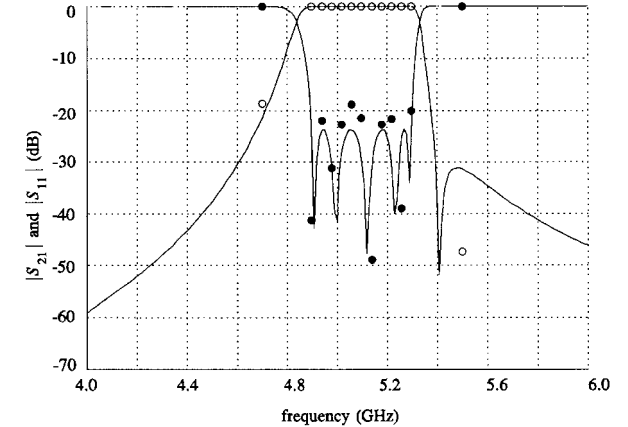
improved and the bandwidth has been reduced on the lower frequency side.

Another SM iteration is performed. The fine-model EM simulation results are shown in Fig. 10. It shows further improvement over the results of the first iteration.

Table II tracks the points in the X_{os} space, showing the Euclidian distance between the point $x_{\text{os}}^{(i)}$ and the optimal

TABLE III
ITERATIONS IN THE X_{em} SPACE

	x_1	x_2	x_3	x_4	x_5	x_6
$x_{em}^{(1)}$	13	27	7	28	25	30
$x_{em}^{(2)}$	13	27	7	28	28	33
$x_{em}^{(3)}$	13	27	7	28	28	34

All values shown are in mils.
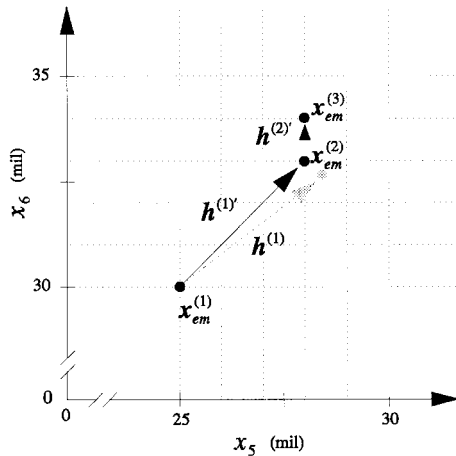
Fig. 11. Illustration of snapping the fine-model parameters to the grid.

Fig. 12. Fine-model EM simulation at $x_{\text{em}}^{(3)}$ using a fine frequency sweep.

point x_{os}^{*}. Table III shows the progress in the X_{em} space. Notice that in the step from $x_{\text{em}}^{(2)}$ to $x_{\text{em}}^{(3)}$, only one variable, namely x_6, has changed by just 1 mil. It indicates a rapid convergence, demonstrating the benefits of the penalty function approach.

As described in (10) and (11), the fine-model parameter values are snapped to the nearest on-grid point during the SM process in order to avoid extra EM simulations of the fine model. This is illustrated in Fig. 11.

C. Selection of Frequency Points

In the coarse model simulation, the 12-port substructure and the vias are analyzed by *em* at 51 frequency points. For the fine-model EM simulation, one obviously wishes to use as few frequency points as possible to save CPU time. The selected frequency points should provide enough information for aligning the models and establishing the mapping between X_{os} and X_{em}. Generally, this requires much fewer frequency points than would be needed for producing a smooth plot of the responses over the whole frequency band. In Figs. 7–10, for the fine-model EM simulation, 11 frequency points are chosen in the passband, one frequency point in the upper stopband and another one in the lower stopband.

To verify the SM solution obtained using the selected few frequency points, EM simulation of the fine model is performed at $x_{\text{em}}^{(3)}$ with 43 frequency points. The results are shown in Fig. 12. The passband return loss is better than 18.5 dB and the insertion loss ripples are less than 0.1 dB.
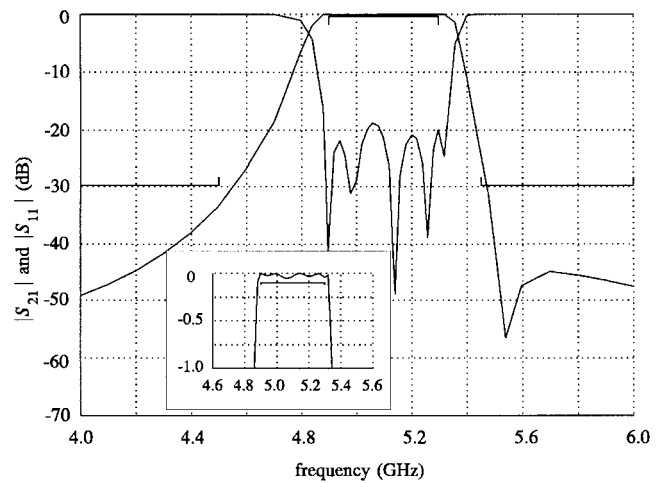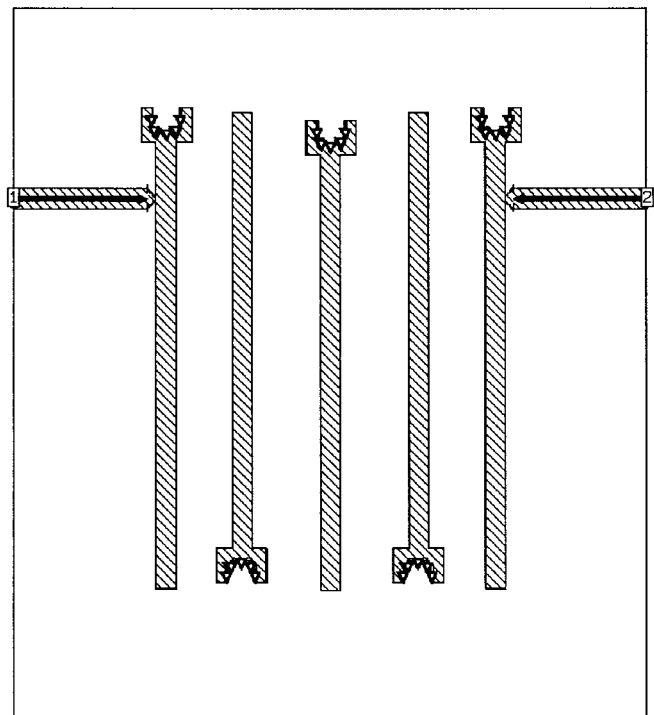

Fig. 13. Filter after cutting off the metal areas with nearly zero current.

D. Consideration of Losses

In order to include dielectric and conductor losses in EM simulation while keeping the increase in CPU time to a minimum, an attempt is made to simplify the geometry by cutting away any redundant metal which does not contribute to the EM-simulation result. Swanson [11] has shown that the current density plots produced by *em* and *emvu* [18] can provide useful information in this regard. It can be seen from such plots that the current density on the outside edges of the vias is nearly zero. The EM simulation can be sped up by cutting off those areas, as shown in Fig. 13. Fig. 14 compares the filter responses before and after this modification and shows only minor differences.
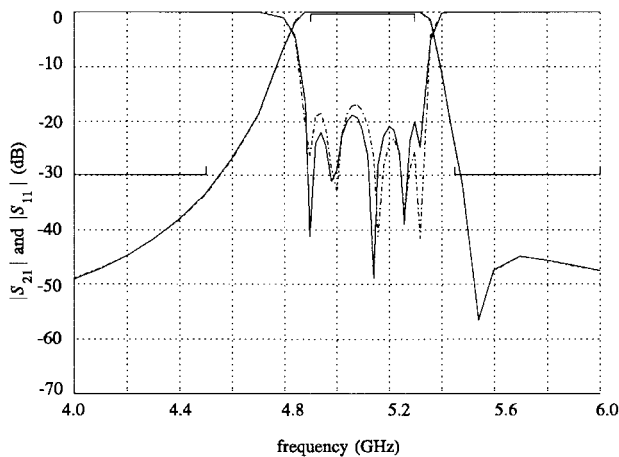
Fig. 14.   Comparison of the filter responses before (solid lines) and after (dotted lines) cutting off the metal areas with nearly zero current.
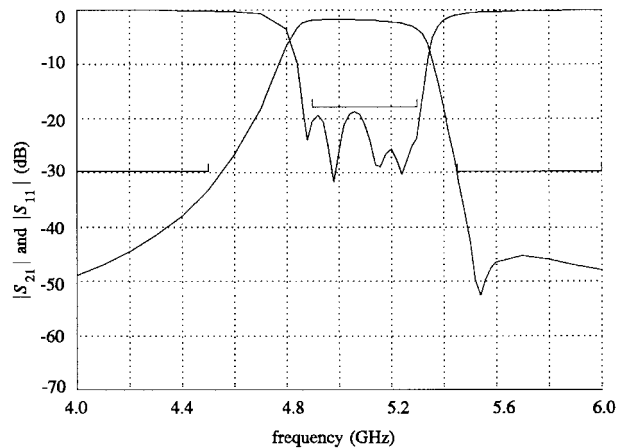

Fig. 15.   The filter responses with dielectric and conductor losses.

Fig. 15 shows the filter responses with the dielectric and conductor losses included in the EM simulation and with the redundant metal removed. The substrate loss tangent is set to 0.001 and the copper conductivity is assumed to be 5.8×10^7. All the specifications are satisfied. The passband return loss is better than 18.5 dB.

V. CONCLUSION

A new design methodology for EM optimization has been presented. A coherent framework has been developed to combine the power of the aggressive SM strategy and the decomposition technique. An intelligent decomposition approach has enabled the authors to construct highly efficient coarse models to carry out the bulk of the computational loads speedily. With a few carefully aligned fine-model simulations, the authors were able to map the optimal solution from the coarse model space into the fine-model space.

A penalty function has been introduced in the parameter extraction process to improve the uniqueness of the solution and the convergence of the SM process.

This new approach has been demonstrated through the EM design optimization of an interdigital filter. The results have shown that rapid and significant improvements have been

achieved after each iteration. A properly aligned design with desirable responses has been obtained after just three fine-model EM simulations. Furthermore, only 13 frequency points were needed for the fine-model simulation—far fewer than would have been needed for a direct optimization of the fine-model responses over the same frequency band. In fact, the total EM simulation effort in the design is equivalent to a single fine-model EM simulation with 39 frequency points. It means that with a proper strategy one can execute EM optimization of practical designs with essentially the same magnitude of effort as that of a detailed EM simulation.

The SM concept can be extended to include as the *ultimate* fine model a production prototype, the responses of which are obtained by measurement. A mapping established iteratively between a coarse simulation model and the device under test will not only guide optimization of the design but also provide invaluable insight into post-production tuning and further refinement of the simulation model.

REFERENCES

[1] J. T. Bolljahn and G. L. Matthaei, "A study of the phase and filter properties of arrays of parallel conductors between ground planes," *Proc. IRE,* vol. 50, pp. 299–311, Mar. 1962.

[2] G. L. Matthaei, "Interdigital band-pass filters," *IEEE Trans. Microwave Theory Tech.,* vol. MTT-10, pp. 479–491, Nov. 1962.

[3] R. J. Wenzel, "Exact theory of interdigital band-pass filters and related coupled structures," *IEEE Trans. Microwave Theory Tech.,* vol. MTT-13, pp. 559–575, Sept. 1965.

[4] E. G. Cristal, "Tapped line coupled transmission lines with applications to interdigital and combine filters," *IEEE Trans. Microwave Theory Tech.,* vol. MTT-23, pp. 1007–1012, Dec. 1975.

[5] J. S. Wong, "Microstrip tapped-line filter design," *IEEE Trans. Microwave Theory Tech.,* vol. MTT-27, pp. 44–50, Jan. 1979.

[6] R. F. Harrington, *Field Computation by Moment Methods.*   New York: Macmillan, 1968.

[7] J. C. Rautio and R. F. Harrington, "An electromagnetic time-harmonic analysis of shielded microstrip circuits," *IEEE Trans. Microwave Theory Tech.,* vol. MTT-35, pp. 726–730, Aug. 1987.

[8] K. Ise, K. Inoue, and M. Koshiba, "Three-dimensional finite-element method with edge elements for electromagnetic waveguide discontinuities," *IEEE Trans. Microwave Theory Tech.,* vol. 39, pp. 1289–1295, Aug. 1991.

[9] W.-T. Lo and C.-K. C. Tzuang, "K-band quasiplanar tapped combline filter and diplexer," *IEEE Trans. Microwave Theory Tech.,* vol. 41, pp. 215–223, Feb. 1993.

[10] D. G. Swanson, Jr., R. Forse, and B. J. L. Nilsson, "A 10-GHz thin film lumped element high temperature superconductor filter," in *IEEE MTT-S Int. Microwave Symp. Dig.,* Albuquerque, NM, June 1992, pp. 1191–1193.

[11] D. G. Swanson, Jr., *Microstrip filter design using electromagnetics,* Santa Clara Valley MTT Short Course: CAD For Modern Microwave Systems, Apr. 1995.

[12] J. W. Bandler, R. M. Biernacki, S. H. Chen, P. A. Grobelny, and R. H. Hemmers, "Space mapping technique for electromagnetic optimization," *IEEE Trans. Microwave Theory Tech.,* vol. 42, pp. 2536–2544, Dec. 1994.

[13] J. W. Bandler, R. M. Biernacki, S. H. Chen, R. H. Hemmers, and K. Madsen, "Electromagnetic optimization exploiting aggressive space mapping," *IEEE Trans. Microwave Theory Tech.,* vol. 43, pp. 2874–2882, Dec. 1995.

[14] M.-Q. Lee and S. Nam, "Efficient coupling patterns design of miniaturized dielectric filter using EM simulator and EPO technique," in *IEEE MTT-S Int. Microwave Symp. Dig.,* San Francisco, CA, June 1996, pp. 737–740.

[15] C. G. Broyden, "A class of methods for solving nonlinear simultaneous equations," *Math. Comput.,* vol. 19, no. 92, pp. 577–593, Oct. 1965.

[16] J. W. Bandler and S. H. Chen, "Circuit optimization: The state of the art," *IEEE Trans. Microwave Theory Tech.,* vol. 36, pp. 424–443, Feb. 1988.

[17] J. W. Bandler, S. H. Chen, R. M. Biernacki, L. Gao, K. Madsen, and H. Yu, "Huber optimization of circuits: A robust approach," *IEEE Trans. Microwave Theory Tech.,* vol. 41, pp. 2279–2287, Dec. 1993.

[18] *em* and *emvu*, Sonnet Software, Inc., Liverpool, NY.

[19] $OSA90/hope^{\text{TM}}$ and $Empipe^{\text{TM}}$, Optimization Systems Associates, Inc., Dundas, Ont., Canada.

[20] G. L. Matthaei, L. Young, and E. M. T. Jones, *Microwave Filters, Impedance-Matching Networks, and Coupling Structures.* New York: McGraw-Hill, 1964, ch. 10.

[21] D. G. Swanson, Jr., *EM field-simulator applications in practical circuit design,* Two Day Short Course, Besser Associates, Los Altos, CA, Jan. 1996.

Shao Hua Chen (S'84–M'85–SM'95) was born in Swatow, China, on September 27, 1957. He received the B.S. Eng. degree from the South China Institute of Technology, Guangzhou, China, in 1982 and the Ph.D. degree in electrical engineering from McMaster University, Hamilton, Ont., Canada, in 1987.

From July 1982 to August 1983, he was a Teaching Assistant in the Department of Automation, South China Institute of Technology. He joined Optimization Systems Associates, Inc., Dundas, Ont., Canada, in 1987 and has been engaged in commercial CAD software development. He has made major contributions to the development of OSA's commercial CAD software systems. He is currently working as a Senior Research Engineer in the Simulation Optimization Systems Research Laboratory, McMaster University. He is also a Senior Consulting Engineer with OSA. He is the author of over 65 papers. His professional interests include optimization theory and implementation, analog circuit simulation, device modeling, statistical design centering, electromagnetic analysis and optimization, software engineering, computer graphics, and CAD framework architecture.

John W. Bandler (S'66–M'66–SM'74–F'78), for a photograph and biography, see this issue, p. 711.

Radoslaw M. Biernacki (M'85–SM'86–F'96) was born in Warsaw, Poland. He received the M.S. and Ph.D. degrees from the Warsaw University of Technology, Warsaw, Poland, in 1969 and 1976, respectively.

He became a Research and Teaching Assistant in 1969 and an Assistant Professor in 1976 at the Institute of Electronics Fundamentals, the Warsaw University of Technology. From 1978 to 1980, he was on leave with the Research Group on Simulation, Optimization, and Control and the Department of Electrical and Computer Engineering, McMaster University, Hamilton, Canada, as a Post-Doctorate Fellow. From 1984 to 1986, he was a Visiting Associate Professor at Texas A&M University, College Station, TX. In 1986, he joined Optimization Systems Associates, Inc., Dundas, Ont., Canada, where he is currently Vice President, Research and Development. He has been involved in the development of all of OSA's commercial CAD software systems, and related research on parameter extraction, statistical device modeling, simulation, and optimization, including yield-driven design of linear and nonlinear microwave circuits, and electromagnetic design optimization. Since 1988, he has been a part-time Professor in the Department of Electrical and Computer Engineering, McMaster University. He conducts research in the Simulation Optimization Systems Research Laboratory. He is the author of over 100 publications. His research interests include system theory, optimization and numerical methods, computer-aided design of integrated circuits, and control systems.

Dr. Biernacki has been the recipient of several prizes for his research and teaching activities.

Ya Fei Huang (M'96) was born in Guizhou, China, in 1963. He received the B.Eng. and Ph.D. degrees from the University of Electronic Science and Technology of China, China, both in electrical engineering, in 1984 and 1990, respectively.

From 1990 to 1993, he was with South China University of Technology, where he conducted research on the applications of high-temperature superconductors in MIC, EM modeling, and filtering. From 1993 to 1995, he was with the University of Saskatchewan as a Post–Doctoral Fellow, where he worked on synthesis, simulation, and optimization of filters and multiplexers for satellite and wireless applications. From 1995 to 1996, he was with McMaster University as a Research Engineer where he worked on design optimization of filters. He then worked for a few months for Com Dev, Ltd. on filter modeling. In 1996, he joined Filtronic Comtek Inc., Salisbury, MD, as a Senior Engineer where he works on filters and multiplexers for wireless applications. His research interests include CAD, EM modeling and simulation, microwave network, and design optimization.